Paper No. 1088. (quote when citing this article)
Eleventh World Conference on Earthquake Engineering
ISBN: 0 08 042822 3

POST LIQUEFACTION CHARACTERISTIC OF SAND

H. KIKU and S. TSUJINO

Engineering Research Institute, Sato Kogyo Co., Ltd.
4-12-20 Nihonbashi-Honcho, Chuo-ku, Tokyo 103, Japan

ABSTRACT

Behavior of sand after liquefaction is discussed and formulated. Material properties that are usually assumed constant, such as internal friction angle, is shown to change due to cyclic loading causing liquefaction. It is also shown that regions with very small stiffness appears by the cyclic loading. They may expand several ten percents, which causes liquefaction-induced large permanent displacement. A simplified model is introduced and improved so as to be able to take into new features such as change of material property and appearance of low stiffness region. The agreement of the numerical calculation and test are very good. Future research needs for evaluating the amount of liquefaction-induced permanent displacement more precisely are also pointed out.

KEYWORDS

Soil Liquefaction; Large Ground Displacement; Constitutive Model; Numerical Calculation; Laboratory Test.

INTRODUCTION

Since Hamada *et al.* (1986) found that large permanent displacement (lateral spreading) occurred when soil liquefied in a widespread area, many efforts have been done to find the mechanism of lateral spreading caused by liquefaction and to evaluate the amount of lateral spreading (Hamada *et al.*, 1994). Through the studies such as shaking table test (Yasuda *et al.*, 1992) and investigation of piles damaged due to lateral spreading (Yoshida *et al.*, 1990), it have been clarified that large deformation occurs in whole liquefied layer but not in a particular slip line. Then, several analytical methods have been proposed for predicting the magnitude of lateral spreading based on the mechanism (Yoshida, 1990 and Yasuda *et al.*,1992). Yoshida used equivalent linear concept in the FEM analysis. Yasuda used additional simplification, small deformation theory, in addition to linear stress-strain relationship. In these analyses, stiffness of liquefied

layer is assumed to be very small. In this paper, we discuss the behavior of sand at large strains and that after the liquefaction from the point of view for developing the stress-strain model based on test result.

REVIEW OF LABORATORY TEST AFTER LIQUEFACTION

Torsional shear tests on the behavior of Toyoura sand after liquefaction are conducted (Kiku, 1994). Fig. 1 shows loading program schematically. After isotropic consolidation, cyclic load is applied until the safety factor against liquefaction, FL, decreases to a prescribed value under an undrained condition. Finally, load is applied so that shear strain increases monotonically. Only the behavior at the monotonic loading stage is shown and discussed hereafter. Fig. 2(a) shows examples of test result. Here, "static" indicates the test in which there is no cyclic load before monotonic loading. Big difference is seen between the results of static and the of other loadings (called "post-liquefaction loading" hereafter). Shear stress at the beginning of the monotonic loading is nearly zero in the post-liquefaction loading. Fig. 2(b) focuses on the behavior at small stresses. The stiffness at the beginning of loading is very small, but not zero although loading starts after the soil liquefied. At certain strain, the sand recovers its stiffness very rapidly, and, as seen in Fig. 2(a), stiffness finally becomes comparable order with the one of static loading. The former part is called low stiffness region and the latter high stiffness region hereafter. Our goal is to predict the behavior of sand in whole these region.

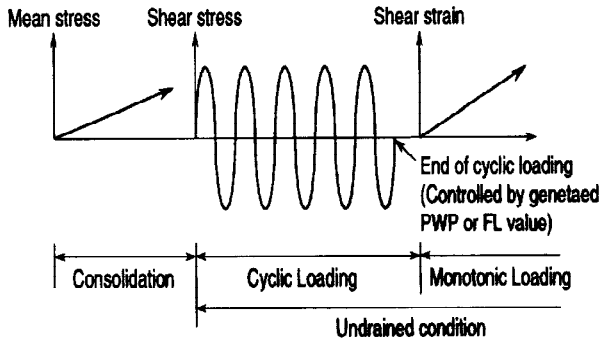

Fig. 1 Loading Program

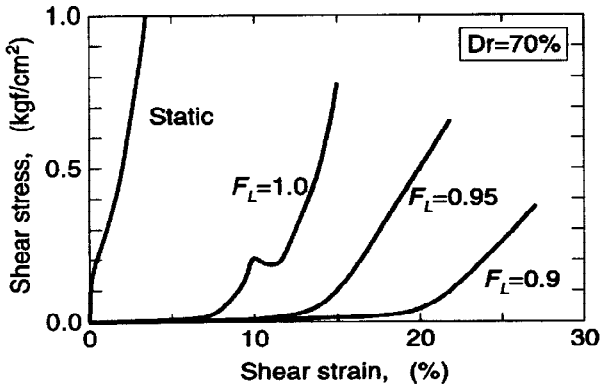

(a) Whole test result

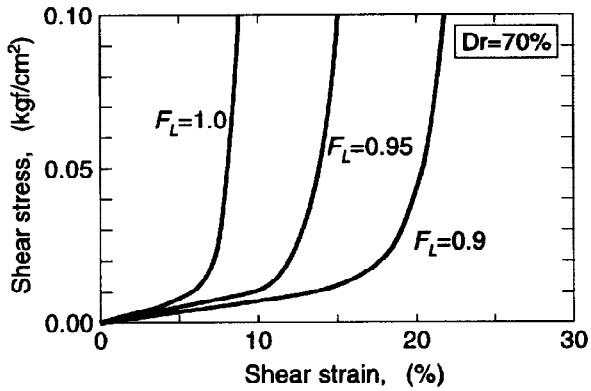

(b) Behavior at small stress

Fig.2 Stress-strain relation of typical test results

STRESS-STRAIN MODEL ON SAND POST LIQUEFACTION

Basic Equations of Stress-Strain Model

A simplified method (Yoshida *et al.*, 1993a,b) is employed for formulating the basic stress-strain model. Although this method includes wide scope including cyclic plasticity, the simplest form is used so as to make the characteristics of the behavior of sand clear. Deformation of soil is divided into volume change and shear deformation. Incrementally elastic behavior is assumed for the volume change;

$$dp' = Kd(\varepsilon_v - \varepsilon_{vd}) \quad (1)$$

$$K=K_0 p'^n \quad (2)$$

where, p' effective mean stress; K tangent bulk modulus; K_0 bulk modulus constant; n bulk modulus

exponent; ε_v volumetric strain; ε_{vd} volume change due to dilatancy.

Volume change ε_{vd} due to dilatancy is computed by using the generalized stress-dilatancy relationship,

$$\frac{d\varepsilon_{vd}}{d\gamma} = \mu - \frac{\tau}{p'} \tag{3}$$

where γ denotes equivalent shear strain, and τ denotes equivalent shear stress (*radius of Mohr's cycle*). The variable μ is a parameter, but, at present, we put $\mu=\mu_p$ following the ordinary stress-dilatancy relationship, where and μ_p denotes stress ratio τ/p' at phase transform. From Eqs. 1 and 3, we can compute effective mean stress increment for given strain increment $d\varepsilon_{ij}$. Therefore, the value of effective mean stress is known when computing shear deformation in the followings. Hyperbolic model is employed for shear stress-shear strain relationship, which is expressed in the dimensionless form as

$$\eta = \frac{\xi}{1+\xi} \tag{4}$$

$$\tau_{max}=p'\sin\phi \tag{5}$$

where, $\eta=\tau/\tau_{max}$ shear stress ratio; τ_{max} shear strength; ϕ internal friction angle; G_{max} shear modulus at small strains; $\xi = \frac{\gamma G_{max}}{\tau_{max}}$ shear strain ratio.

Since effective mean stress is already known, both G_{max} and τ_{max} are known quantities. Dimensionless tangent shear modulus γ is obtained by differentiating η with respect to ξ, which yields

$$g = \frac{d\eta}{d\xi} = \frac{1}{(1+\xi)^2} \tag{6}$$

Finally, deviatoric stress increment ds_{ij} is obtained from the given deviatoric strain increment $d\gamma_{ij}$ as

$$ds_{ij} = gG_{max}d\gamma_{ij} \tag{7}$$

Stress increment is computed from Eqs. 1 and 7.

This formulation is shown to be effective for simulating the behavior of sand in the ordinary shear strain range up to several percent (Yoshida *et al.*, 1993b). However, it does not seem to be valid at very large strains or for the behavior after liquefaction, which will be discussed hereafter. The formulation will be improved based on the discussion of the characteristics of the behavior of sand both at large strains and after the liquefaction.

Behavior of Sand at Large Strains

Equivalent shear strain increment $d\gamma$ is easily computed from a given strain increment $d\varepsilon_{ij}$. Then, volumetric change due to dilatancy is computed from Eq.3. Under the undrained condition, however, this volume change does not occur, but effective mean stress changes by the amount of

$$dp' = -Kd\varepsilon_{vd} \tag{8}$$

Substitution of Eq.3 into Eq.8 yields

$$dp' = K(\frac{\tau}{p'} - \mu)d\gamma \tag{9}$$

Since the stress path moves along the failure surface, the stress ratio τ/p' is approximately expressed as

$$\frac{\tau}{p'} = \sin\phi \tag{10}$$

Therefore, Eq.9 yields

$$dp' = K(\sin\phi - \mu)\, d\gamma \tag{11}$$

Shear strength increment $d\tau_{max}$ during the change of mean effective stress is computed from Eq. 5 as

$$d\tau_{max}=dp'\sin\phi \tag{12}$$

We again use the assumption that stress path moves along the failure surface. Then, equivalent shear stress increment $d\tau$ is nearly equals to the shear strength increment $d\tau_{max}$. Finally, we obtain stress-strain relationships at large strains in the incremental form

$$d\tau = K(\sin\phi-\mu)\sin\phi\cdot d\gamma \tag{13}$$

Eq.13 implies that a computed stiffness at large strains is strongly affected by the value of μ, because other parameters are well known physical quantities. The value of μ for static loading is back calculated from Eq. 13 and $d\tau/dp'$ value read off from the test result. Here tangent bulk modulus is computed from

$$K=\frac{2(1+\nu)}{3(1-2\nu)}G_{max} \tag{14}$$

where ν denotes Poisson's ratio. Shear modulus G_{max} at small strains is computed from the empirical equation for Toyoura sand (Kokusho, 1980),

$$G_{max}=840\frac{(2.17-e)^2}{1+e}p'^{1/2} \qquad (\mathrm{kgf/cm^2}) \tag{15}$$

where e denotes void ratio. Fig. 3 shows computed μ value at large strains, μ_f. The value of μ increases with relative density. This tendency is quite different with the tendency of phase transformation angle which decreases with relative density. Therefore it is obvious that we cannot obtain good prediction at large strains if $\mu=\mu_p$ is used at large strains. The change of μ value from stress ratio $\eta=\mu_p$ (phase transform) to $\eta=1$ (on failure line) is not known. In the followings, therefore, we use piecewise linear relationship between μ and η. Fig. 4 shows the result of analysis for static loading. The agreement between test and analysis is very good.

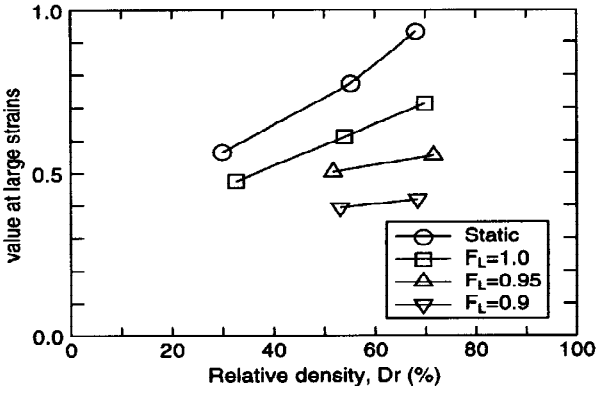

Fig. 3 The value of μ at large strains

Effect of Occurrence of Liquefaction

In almost all constitutive models, material properties with physical meanings such as internal friction angle are assumed to be constant even if liquefaction occurs. As the first trial, therefore, we use similar method; the effect of liquefaction is considered only in the initial condition. Because of the occurrence of liquefaction, effective mean stress decreases very much. So, we use 1/100 of initial effective mean stress, p_0=0.005kgf/cm^2, as initial mean stress.

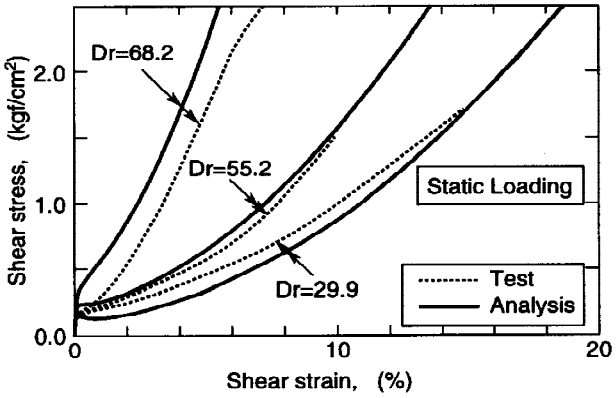

Fig. 4 τ-γ relationship for static loading

After analyses, observation of both test result and detailed comparison between test and analysis show following disagreements.

1) Analysis shows larger stiffness at the beginning of loading, because low stiffness region observed in the test is not considered in the analysis.

2) Stiffness at high stiffness region by test decreases depending of FL, but constant in the analysis.

3) The behavior of post-liquefaction loading changes depending on FL value, but it is not considered in the

analysis.

These facts imply that material property may change during the cyclic loading conducted before the post-liquefaction loading. In the following sections, we will discuss these and consider the effect of liquefaction in developing the stress-strain modeling.

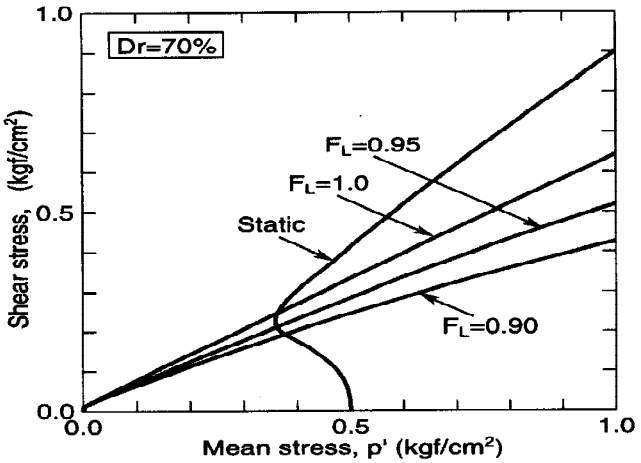

Fig. 5 Stress path of test with relative density of 70%

Internal Friction Angle and Phase Transform

Fig.5 shows an example of stress paths of the test of relative density 70%. The stress-strain relationship of this test is shown in Fig. 2. Stress path moves linearly after phase transformed for static loading test. It moves almost linearly from the beginning of loading for post-liquefaction loading test. Therefore, stress point is supposed to move along the failure line. It is clearly observed that the slope decreases with FL value, which implies that internal friction angle changes depending on the loading before the monotonic loading.

The slope angles are read from stress path trajectory and plotted in Fig. 6. Those obtained from tests with other relative densities are also plotted in the figure. Here, it is noted that this angle is not an internal friction angle ϕ, but $\tan^{-1}(\sin\phi)$. The dependency of internal friction angle on the loading before liquefaction is also clearly observed. Phase transform is very difficult or impossible to read from test result of post-liquefaction loading. According to the parametric studies using the final form of the stress-strain model of this paper, however, μ_p value does not affect the whole behavior very much. Therefore, in the following analysis, it is held constant regardless of FL value. Knowing the internal friction angle and the slope of the stress-strain curve at high stiffness region, the value of μ_f can be calculated. The result is overplotted in Fig. 3. The value of μ_f decreases as FL value decreases or cyclic loading after liquefaction increases, which is the similar to the tendency of internal friction angle.

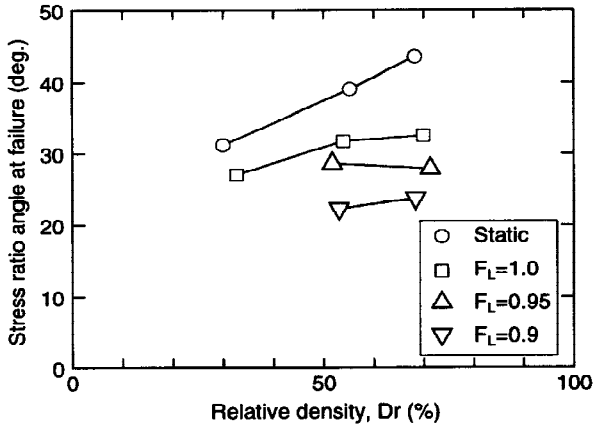

Fig.6 Change of slope of failure line caused by liquefaction

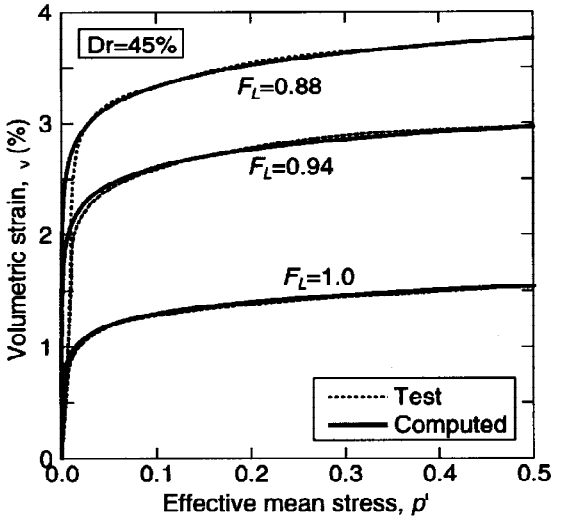

Fig. 7 Volumetric strain characteristics during the excess pore water pressure dissipation after liquefaction.

Evaluation of Low Stiffness Region

It is easily recognized from the previous analysis that modification of internal friction angle and μ value will improve the behavior in high stiffness region, but not in low stiffness region. Yoshida *et al.* (1994) measured the relationship between the volumetric strain and effective mean stress during the process of

excess pore water pressure dissipation so as to obtain the settlement characteristics of the ground after liquefaction by means of triaxial shear test apparatus. Figure 7 shows typical result of the test.

The p'-ε_v relationship is divided into two parts. At the beginning of drainage, bulk modulus is very small. It increases very rapidly at certain volumetric strain. This behavior is similar to the test result described in the previous section; low stiffness region and high stiffness region correspond to low and high bulk modulus regions, respectively. The p'-ε_v relationship shown in Fig. 7 is obtained on the process of excess pore water pressure dissipation. If principle of effective stress holds, however, the same relationship is valid for the undrained behavior discussed here. Since there is few change of shear strain on the process of drainage, volume change due to dilatancy is supposed not to include in the measured volumetric change in Fig. 7. Yoshida *et al.* (1994) pointed out that bulk modulus at high bulk modulus region is consistent to the bulk modulus derived from ordinary empirical equation such as Eq. 2. This implies that elastic modulus (tangent bulk modulus) is very small in the low bulk modulus region. If so, it is also reasonable to assume that shear modulus G_{max} at small strains is also very small. Otherwise, Poisson's ratio becomes very small or negative, which is not realistic. Yoshida and Finn (1994) formulates the behavior in Fig. 7 in the following equation,

$$\frac{p'}{p'_0} = \frac{e^{\frac{\varepsilon_v}{c}} - 1}{e^{\frac{\varepsilon_{vo}}{c}} - 1} \tag{16}$$

where p'_0 denotes initial effective mean stress from which cyclic load is applied to cause liquefaction, and ε_{vo} denotes a volumetric strain at $p' = p'_0$. The variable c is a parameter, which is expressed as

$$c = 0.053\varepsilon_{vo} + 0.0007 \tag{17}$$

Tangent bulk modulus to be used instead of Eq. 2 is obtained from Eq. 16 as a function of effective mean stress p' as

$$K = \frac{1}{c} \frac{p'_0 - p'(e^{\frac{\varepsilon_v}{c}} - 1)}{e^{\frac{\varepsilon_{vo}}{c}} - 1} \tag{18}$$

The shear modulus G_{max} at small strains is then obtained from Eq. 14, where, in the following analysis, the value of Poisson's ratio is kept constant. In the following analysis, tangent bulk modulus and shear modulus at small strains derived from Eqs. 18 and 14 are used, which covers both low and high stiffness regions. Here, it is noted that ε_{vo} in Eq. 16 was actual value which occurs after excess pore water pressure dissipates, but, when using in the analysis here, it is a fictitious value.

RESULT OF ANALYSIS AND DISCUSSION

In the first part of this paper, we introduced a basic form of stress-strain model, and after that, we have discussed the effect of liquefaction on the behavior of sand at large strains. From the point of view for computing the behavior of soil, they are summarized as follows;

1) Internal friction angle changes during the cyclic loading causing liquefaction.

2) The value of m at phase transform and that at large strains where stress path moves along the failure line are different to each other; the latter is generally larger than the former. Piecewise linear relationship is used in terms of shear stress ratio in this analysis. The value of μ_f is shown in Fig.3, which also changes depending on the amount of cyclic loading.

3) Tangent bulk modulus K is computed from Eq. 18 instead of Eq. 2. Shear modulus G_{max} at small strains

is computed from Eq. 14, where Poisson's ratio is kept constant.

In applying Eq. 18, the value of ε_{vo} is not known, because it can be obtained after excess pore water pressure dissipates. Moreover, since only the test result with relative density of 45% is shown in Fig. 7, ε_{vo} at other relative densities cannot be obtained from the figure. Therefore, we treat ε_{vo} as a fitting parameter.

Fig.8 to 10 show the result of analysis and test result. Here, the value of μ_f cannot be read from the test result of Dr=30% and FL=0.95 and 0.9, therefore suitable value is assumed. The agreement of analysis with test result is very good for both low stiffness region and high stiffness region, although a little disagreement is seen at the transition between two regions.

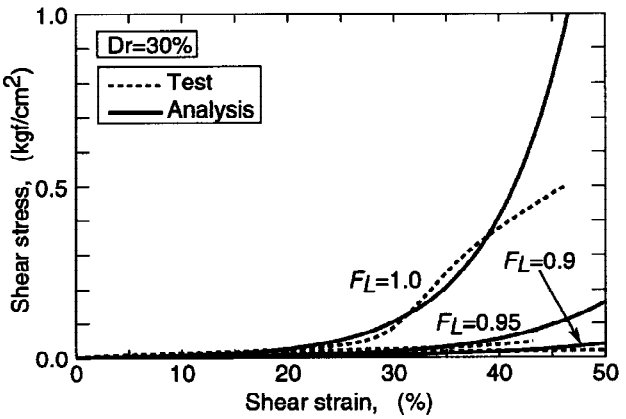

Fig. 8 Stress-strain relationship for Dr=30%

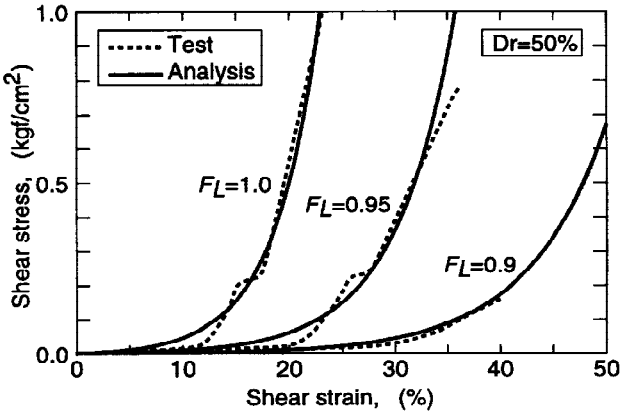

Fig. 9 Stress-strain relationship for Dr=50%

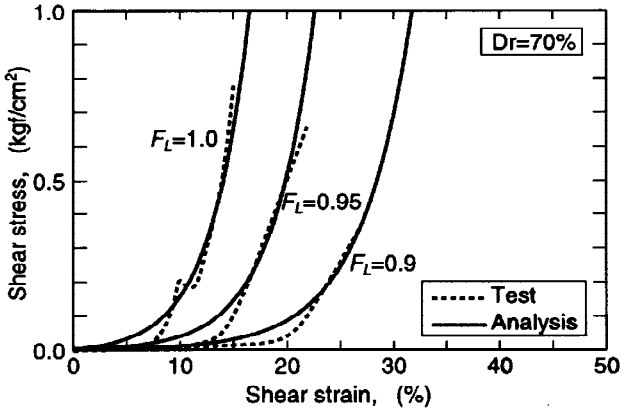

Fig. 10 Stress-strain relationship for Dr=70%

CONCLUSION

Several new features are presented in this paper from the point of view to predict the behavior of sand after liquefaction. The biggest one is the appearance of low stiffness region whose size depends on the amount of cyclic loading. The stiffness of this region is very small, and the strain is as large as several ten percents, which is a sufficient order of shear strain to cause large amount of liquefaction-induced permanent deformation. It may be recognized that this region occurs because soil particle configuration is very unstable, possibly floating up in the pore water or just close to that. The phase change from low stiffness region to high stiffness region occurs because the soil particle comes to a new stable configuration. This concept explains the change of material property due to cyclic loading. Therefore, the mechanism of liquefaction-induced lateral spreading is quite different with the ordinary discussion on residual strength or steady state under monotonic loading without cyclic loading before it. It is also noted that low stiffness region is observed even at FL=1.0. It implies that this stage appears even before the occurrence of liquefaction. However, constitutive models usually does not consider the appearance of this region.

We also showed that the behavior of soil can be computed with reasonable accuracy by considering the low stiffness region. However, some of the parameters were not evaluated well because empirical experience is short or not conducted to evaluate these values within required accuracy. Therefore, we employed relevant

value by our judgment in this paper, which may not be best choice and result in disagreement. However, since it is not expressed in a formula and value at very low confining pressure is not shown, we do not consider p' dependency of Poisson's ratio. The same things occurred for phase transform angle. Moreover, we used Eq. 16 but the validity of this equation is proved only in particular cases. The change of internal friction angle and μ by cyclic loading are also not formulated. Research is required to obtain these behavior and to develop the empirical formulae used in the analysis.

ACKNOWLEDGMENT

This research was conducted under the leadership of Dr. N. Yoshida of Sato Kogyo Co., Unfortunately, because of the limitation of the numbers of author in WCEE, his name cannot be put as author in this paper.

REFERENCES

Hamada,M., Yasuda,S., Isoyama,R. and Emoto,K. (1986): Study on Liquefaction Induced Permanent Ground Displacement, Association for the Development of Earthquake Prediction, Tokyo

Hamada,M, O'Rouke,T.D. and Yoshida,N. (1994): Liquefaction-induced Large Ground Displacement, Performance of Ground and Soil Structures during Earthquakes, 13th ICSMFE, New Delhi, JSSMFE, pp.93-108

Yasuda,S., Nagase,H., Kiku,H. and Uchida,Y. (1992): The mechanism and a simplified procedure for the analysis of permanent ground displacement due to liquefaction, Soils and Foundations, Vol.32, No.1, pp.149-160

Yoshida,N. and Hamada,M. (1990): Damage to Foundation Piles and Deformation Pattern of Ground due to Liquefaction-induced Permanent Ground Deformations, Proc., 3rd Japan-U.S. Workshop on Earthquake Resistant Design of Lifeline Facilities and Countermeasures for Soil Liquefaction, San Francisco, CA

Kiku,H., Yasuda,S., Masuda,T., Itafuji,S. and Mine,K.(1994): Torsional Shear Tests on the Deformation Character of Sand before and after Liquefaction, proc., 9th Japan Earthquake engineering Symposium, Vol.1, pp.871-876 (in Japanese)

Yoshida,N. and Tsujino,S. (1993a): A simplified Practical Stress-strain Model for the Multi-dimensional Analysis under Repeated Loading, Proc., The 28th Japan National Conference of Soil Mechanics and Foundation Engineering, pp.1221-1224 (in Japanese)

Yoshida,N., Tsujino,S., Nakajima,T. and Yano,Y. (1993b): A Simplified Practical Model for the Use of Multi-Dimensional Analysis, Part 2, Consideration of Dilatancy, Proc., 48th Annual Conf. of the Japan Society of Civil Engineering, Vol.3, pp.1218-1219

Kokusho,T. (1980): Cyclic Triaxial Test of Dynamic Soil Properties for Wide Strain Range, Soils and Foundations, Vol.29, No.2, pp.45-60

Yoshida,N. and Finn,W.D.L. (1994) : Joint Element for Liquefaction and Consolidation Analysis (in preparation)

Yoshida,N., Tsujino,S. and Inadomaru,K. (1994): Fundamental Study on the Residual Settlement of Ground after Liquefaction, Proc.,49th Annual Conf. of the Japan Society of Civil Engineering, Vol.3 (in Japanese)